applied optics

Polarization-dependent laser autofluorescence of the polycrystalline networks of blood plasma films in the task of liver pathology differentiation

V. P. Prysyazhnyuk,[1] Yu. A. Ushenko,[2,*] A. V. Dubolazov,[3] A. G. Ushenko,[3] and V. A. Ushenko[2]

[1]The Department of Infectious Diseases and Epidemiology, Bukovinian State Medical University, 2 Theatral Sq., Chernivtsi, Ukraine
[2]Correlation Optics Deptartment, Chernivtsi National University, 2 Kotsiubynskyi St., Chernivtsi, Ukraine
[3]Optics and Publishing Department, Chernivtsi National University, 2 Kotsiubynskyi St., Chernivtsi, Ukraine
*Corresponding author: yuriyu@gmail.com

Current research presents the results of the investigation of diagnostic efficiency of laser polarization autofluorescence for the set of endogenous fluorophores of blood plasma polycrystalline films in two spectral regions (0.5–0.53 µm and 0.63–0.67 µm) under the excitation of laser radiation with a wavelength of 0.405 µm. A model of generalized optical anisotropy of protein networks of blood plasma polycrystalline films is proposed for the purpose of defining laser autofluorescence processes. Both phase (linear birefringence and optical activity) and amplitude (linear and circular dichroisms) anisotropies have been considered. Interconnections between the optimal condition of probing beam polarization state and the efficiency of induction laser autofluorescence have been found. Statistical analysis of coordinate distributions of laser polarization autofluorescence intensities is suggested by means of determination of the quantitative criteria (statistical moments of the 1st–4th orders). The efficiency of laser polarization autofluorescence of polycrystalline networks in the task of differentiation of nonalcoholic fatty liver disease and chronic hepatitis of human liver has been analyzed.   © 2016 Optical Society of America

1. INTRODUCTION

Today, many practical techniques based on measuring and analyzing the Mueller matrices of the investigated samples are being used in biological and medical research [1–10]. Within the past 10–15 years, laser polarimetry has been formed in matrix optics as a separate direction [11–19]. Using this, interconnections between the set of 1st–4th-order statistical moments, correlation and fractal parameters (they characterize the distributions of Mueller matrix elements), and the parameters of linear birefringence of fibrillar protein networks of human biological tissues have been found. The diagnostics of pathological changes of skin derma, epithelial and connective tissues of women's reproductive organs, etc. was realized on this basis [13,15,17,19].

In parallel with polarimetry techniques, methods utilizing the diagnostic application of spectral effects of autofluorescence of biological tissues and molecules are being intensely developed [20–25]. Impressive applied results of using these methods for cancer diagnostics have been obtained.

However, there are practically no data concerning polarization manifestations of autofluorescence effects in biological tissues and fluids in modern literature. Therefore, the task of complex investigation of the diagnostic efficiency of both methods of laser polarimetry and laser autofluorescence proves to be topical.

In this research, the model of complex optical anisotropy, possessed by polycrystalline networks of blood plasma films, is proposed. Furthermore, the method of laser polarization fluorescence in the differentiation of nonalcoholic fatty liver disease and chronic hepatitis of human liver is developed.

Liver biopsy is a "gold standard" of differential diagnostics of chronic diffuse liver diseases. [26,27]. However, this method has a number of limitations and drawbacks such as diagnostic errors in the process of sampling and subjective perception of histological changes. The conventional method of biopsy is painful for patients and exposes the risk of complications such as internal bleeding and the possibility of a secondary infection [28,29]. Therefore, an important task of modern hepatology consists of the search for new noninvasive methods of objectification of pathological processes in the liver. At the same time, the creation of open, low-cost screening and an express method

of diagnostics of the severity of liver disease with an accuracy close to the gold standard remains as one of the objectives.

2. THEORY OF THE METHOD

The description of laser polarization autofluorescence of blood plasma polycrystalline films is based on the following optical model. The formation of laser polarization autofluorescence of the polycrystalline network of blood plasma polycrystalline films is based on the mechanisms of optically anisotropic absorption (linear and circular dichroism) and the mechanisms of phase anisotropy (linear and circular birefringence), which modulate the secondary radiation of biological molecules and their structures.

A. Mechanisms of Optical-Anisotropic Absorption (Amplitude Anisotropy)

Optical peculiarities of linear dichroism are quite completely described by the following Mueller matrix [7,8,10]:

$$\{A\} = \begin{Vmatrix} 1 & a_{12} & a_{13} & 0 \\ a_{21} & a_{22} & a_{23} & 0 \\ a_{31} & a_{32} & a_{33} & 0 \\ 0 & 0 & 0 & a_{44} \end{Vmatrix},$$

where

$$a_{ik} = \frac{1}{1 + \Delta\eta} \times \begin{cases} a_{12} = a_{21} = (1 - \Delta\eta)\cos 2\rho, \\ a_{13} = a_{31} = (1 - \Delta\eta)\sin 2\rho, \\ a_{22} = (1 + \Delta\eta)\cos^2 2\rho + 2\sqrt{\Delta\eta}\sin^2 2\rho, \\ a_{23} = a_{32} = (1 - \Delta\eta)^2 \cos 2\rho \sin 2\rho, \\ a_{33} = (1 + \Delta\eta)\sin^2 2\rho + 2\sqrt{\Delta\eta}\cos^2 2\rho, \\ a_{44} = 2\sqrt{\Delta\eta}. \end{cases}$$

(1)

Here $\Delta\eta = \frac{\eta_x}{\eta_y}$, $\begin{cases} \eta_x = \eta\cos\rho; \\ \eta_y = \eta\sin\rho \end{cases}$, and η_x, η_y are absorption coefficients of the light beam amplitude linearly polarized orthogonal components.

The presence of complex spiral-like molecular protein structures or their combination forms circular dichroism. Optical peculiarities of this mechanism are characterized by the following Mueller matrix:

$$\{F\} = \begin{Vmatrix} 1 & 0 & 0 & f_{14} \\ 0 & f_{22} & 0 & 0 \\ 0 & 0 & f_{33} & 0 \\ f_{41} & 0 & 0 & 1 \end{Vmatrix},$$

where

$$f_{ik} = \begin{cases} f_{22} = f_{33} = \frac{1 - C^2}{1 + C^2}; \\ f_{14} = f_{41} = \pm\frac{2C}{1 + C^2}. \end{cases}$$

(2)

Here, $C = \frac{j_\otimes - j_\oplus}{j_\otimes + j_\oplus}$, and $j_\otimes$, $j_\oplus$ are the indices of absorption of light beam amplitude left-($\otimes$) and right-($\oplus$) circularly polarized components.

B. Mechanisms of Phase Anisotropy

The optical activity of molecular protein structures is characterized by the matrix operator of the following form [19]:

$$\{\Theta\} = \begin{Vmatrix} 1 & 0 & 0 & 0 \\ 0 & \theta_{22} & \theta_{23} & 0 \\ 0 & \theta_{32} & \theta_{33} & 0 \\ 0 & 0 & 0 & 1 \end{Vmatrix},$$

(3)

where $\theta_{ik} = \begin{cases} \theta_{22} = \theta_{33} = \cos 2\omega, \\ \theta_{23} = -\theta_{32} = \sin 2\omega. \end{cases}$

Here, ω is the rotation angle of the polarization plane.

Polycrystalline networks possess linear birefringence and are quite completely described by the Mueller matrix

$$\{H\} = \begin{Vmatrix} 1 & 0 & 0 & 0 \\ 0 & h_{22} & h_{23} & h_{24} \\ 0 & h_{32} & h_{33} & h_{34} \\ 0 & h_{42} & h_{43} & h_{44} \end{Vmatrix}, \quad \text{where}$$

$$h_{ik} = \begin{cases} h_{22} = \cos^2 2\rho + \sin^2 2\rho \cos\phi, \\ h_{23} = h_{32} = \cos 2\rho \sin 2\rho(1 - \cos\phi), \\ h_{33} = \sin^2 2\rho + \cos^2 2\rho \cos\phi, \\ h_{24} = -h_{42} = \sin 2\rho \sin\phi, \\ h_{34} = -h_{43} = \cos 2\rho \sin\phi, \\ h_{44} = \cos\phi. \end{cases}$$

(4)

Here, ρ is the direction of fibrils packing (fast axis orientation), and ϕ is the phase shift between the light beam amplitude linearly polarized orthogonal components.

The mechanisms of optically anisotropic absorption [relation Eqs. (1) and (2)], that determine the laser autofluorescence, sufficiently depend on the optical radiation wavelength and are strongly revealed in the ultraviolet part of the spectrum [20–25]. In the visible part of spectrum, the mechanism of linear dichroism [relation Eqs. (1) and (2)] with the following linear birefringence [relation Eqs. (3) and (4)] is principal. As a result, the following relation takes place:

$$\phi, \Delta\eta \gg \omega, C. \tag{5}$$

It follows from condition Eq. (5) that the matrix operator characterizing the mechanisms of linear dichroism and birefringence of polycrystalline networks can be written as

$$\{P\} = \{H\}\{A\} = \begin{Vmatrix} 1 & P_{12} & P_{13} & P_{14} \\ P_{21} & P_{22} & P_{23} & P_{24} \\ P_{31} & P_{32} & P_{33} & P_{34} \\ P_{41} & P_{42} & P_{43} & P_{44} \end{Vmatrix}. \tag{6}$$

The process of laser radiation absorption and the secondary phase modulation of fluorescence of different types of molecules can be described by the following matrix equation:

$$S^* = \{P\}S(\alpha_0). \tag{7}$$

In the developed form, the Stokes vector of the beam S^* transformed by the object is written as

$$S^* = (1 + P_{12} + P_{13})^{-1} \begin{pmatrix} 1 \\ P_{21} + P_{22}\cos 2\alpha_0 + P_{23}\sin 2\alpha_0 \\ P_{31} + P_{32}\cos 2\alpha_0 + P_{33}\sin 2\alpha_0 \\ P_{41} + P_{42}\cos 2\alpha_0 + P_{43}\sin 2\alpha_0 \end{pmatrix},$$

(8)

where

$$\alpha^* = 0.5 \, \text{arctg} \left(\frac{P_{31} + P_{32} \cos 2\alpha_0 + P_{33} \sin 2\alpha_0}{P_{21} + P_{22} \cos 2\alpha_0 + P_{23} \sin 2\alpha_0} \right), \quad \textbf{(9)}$$

$$\beta* = 0.5 \, \text{arcsin} \left(\frac{P_{41} + P_{42} \cos 2\alpha_0 + P_{43} \sin 2\alpha_0}{1 + P_{12} + P_{13}} \right). \quad \textbf{(10)}$$

Here α^* is the azimuth, and β^* is the polarization ellipticity of the beam transformed by the object.

From the analysis of Eqs. (8)–(11) it follows that by changing of the polarization azimuth α_0 of the illuminating beam it is possible to maximize the impact of linear dichroism. It is easy to show that the fulfillment of the condition

$$\alpha_0^* = \rho \pm 0.25\pi \rightarrow \Delta\eta = 1 \quad \textbf{(11)}$$

transforms the matrix $\{A\}$ [relation Eq. (1)] into a diagonal one $\{a_{ii} = 1\}$.

The decrease of polarization ellipticity becomes the indicator of condition Eq. (16) realization

$$\beta_{\min}^* = 0,5 \, \text{arcsin}(h_{42} \cos 2\alpha_0^* + h_{43} \sin 2\alpha_0^*). \quad \textbf{(12)}$$

On the other hand, physical condition Eq. (12) can be realized in the red part of the spectrum.

Thus, by means of measuring the elements of matrix operator $\{H(\lambda = 0.63 \, \mu m)\}$ in the red part of the spectrum, it is possible to determine the optimal condition of the polarization state of the probing laser beam in the blue part of spectrum.

The following topical tasks should be addressed:

• analysis of the effectiveness of the conventional method of polarization mapping in the "red" ($\lambda = 0.63 \, \mu m$) range of the spectrum, and
• determination of the diagnostic effectiveness of the method of laser polarization autofluorescence $I(\alpha_0^*)$ on the base of Eq. (11).

3. OBJECTS, INVESTIGATION TECHNIQUES, AND PROCESSING ALGORITHMS

In the planning of experimental polarimetric investigations, we used the known data about the formation of the autofluorescence spectrum of blood plasma when it is excited by "blue" ($\lambda = 0.405 \, \mu m$) radiation [25]. There are two main ranges (0.5–0.53 μm and 0.63–0.67 μm) where fluorescence maxima are localized. It should be noted that the nature of these maxima is associated with the simultaneous superposition of the contributions of various endogenous fluorophores: flavoproteins, vitamins, bilirubin, lipoproteins, and porphyrins. However, the fluorescence of each of them has its spectral peaks, which are located in the ranges of $\lambda = 0.510 \, \mu m$ and $\lambda = 0.632 \, \mu m$. As the main object of the comparative experimental studies of plasma films, we have chosen a spectral maximum in the "red" ($\lambda = 0.632 \, \mu m$, domination of porphyrins radiation) range of autofluorescence [23]. However, in any spectral range the aliasing of radiations of different fluorophores takes place. Therefore, as an additional criterion for the differentiation of fluorescence polarization of plasma samples we have chosen another spectral peak (domination of radiation of flavoproteins, vitamins, bilirubin, and lipoproteins). In addition, excitation of plasma fluorescence by "blue" ($\lambda = 0.405 \, \mu m$) radiation provides almost complete elimination

of protein fluorescence (the absorption of proteins is localized in the ultraviolet region) from this process.

Therefore, the main role of polycrystalline networks of plasma proteins is in the secondary phase of modulation—converting the state of polarization of the fluorescent radiation due to the effects of the optical birefringence [Eqs. (3) and (4)].

As objects of investigation, we have used the optically thin (attenuation coefficient $\tau < 0.1$) polycrystalline films of blood plasma of the following three types:

• healthy donors—**group 1** (53 samples),
• nonalcoholic fatty liver disease—**group 2** (53 samples), and
• chronic hepatitis—**group 3** (53 samples).

The samples of optically thin films of blood plasma (attenuation coefficient $\tau < 0.1$) were formed under identical conditions by placing a drop of blood plasma on optically homogeneous glass. The resulting film was dried at room temperature for 24 h ($t = 22°C$). This method of sample preparation was used in several studies of polarization and autofluorescence properties of blood plasma [30–32]. It was shown that they are stable for at least 72 h.

The coordinate distributions of polarization ellipticity in the plane of laser images of polycrystalline films of blood plasma were measured in the setup of the standard Stokes polarimeter [12,13].

The optical scheme of the polarimeter is shown in Fig. 1. The following two regimes can be realized in this setup:

• polarization mapping and
• autofluorescence mapping.

A. Polarization Mapping

Samples of blood plasma were illuminated by a parallel beam of a He–Ne laser ($\lambda = 0.6328 \, \mu m$, $W = 5.0 \, mW$) with radius $r = 1 \, mm$. The polarization state generator consists of quarter-wave plates (3 and 5) and a polarizer (4). Images of polycrystalline films of blood plasma by means of strain-free objective (7) were projected into the plane of a photosensitive area ($m \times n = 1280 \times 960$ pixels) of CCD camera (11). The bandpass filter (10) was removed from the setup. The analysis of polycrystalline films of blood plasma images was carried out by means of a polarization state analyzer, which consisted of a polarizer analyzer (9) and a quarter-wave plate (8). As a result, the Stokes vector parameters for every pixel of the biological
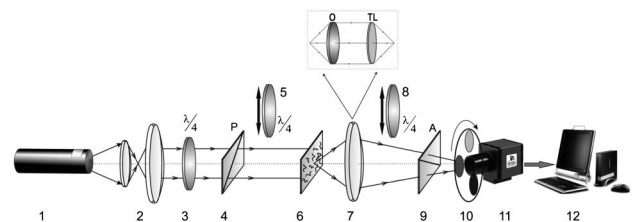

Fig. 1. Optical scheme of the experimental setup. 1, He–Ne laser ($\lambda = 0.6328 \, \mu m$) or blue diode laser ($\lambda = 0.405 \, \mu m$); 2, collimator; 3, 5, and 8, quarter-wave plates; 4 and 9, polarizers; 6, polycrystalline films of blood plasma; 7, imaging node (consists of strain-free objective O and tube lens TL); 10, interference bandpass filter ($\lambda = 630$–670 μm or 500–530 μm); 11, CCD camera; 12, PC.

tissues image $\{S_{i=1,2,3,4}\}$ were calculated. The values of polarization ellipticity within each pixel of CCD camera were calculated as follows:

$$\beta = 0.5 \ \arcsin \ \frac{S_4}{S_1} = 0.5 \ \arcsin \ \frac{I_\otimes - I_\oplus}{I_\otimes + I_\oplus}. \quad \textbf{(13)}$$

Here, $S_{i=1;4}$ is the Stokes vector parameters in the points of the digital image of blood plasma polycrystalline films, and $E_\otimes$, $E_\oplus$ are the intensities of the left- and right-circularly polarized components of the laser beam amplitude.

B. Autofluorescence Mapping

We have used the "blue" diode laser (1) in order to excite the autofluorescence (wavelength $\lambda = 0.405$ µm and power $W = 50$ µW). To perform the spectral separation of polarization autofluorescence, interference filters (10) with transmittance bandpass $\lambda = 630\text{–}650$ µm and $500\text{–}530$ µm were installed before the CCD camera.

Linearly polarized laser beams with polarization azimuths $\alpha_0 = 0°; \ \alpha_0^*$ were used as exciting radiation. For each of these beams, the coordinate distributions of intensity $I(m \times n)$ of laser autofluorescence were registered.

The objective estimation of the coordinate distributions

$$m \equiv \begin{cases} \beta(m \times n) \\ I(m \times n) \end{cases}$$ was performed by means of the methods of

statistical [19] analysis.

The set of statistical moments of the 1st–4th orders characterizing the distributions m was calculated as follows:

$$R_1 = \frac{1}{N} \sum_{j=1}^{N} |m|_j,$$

$$R_2 = \sqrt{\frac{1}{N} \sum_{j=1}^{N} (m - R_1)_j^2},$$

$$R_3 = \frac{1}{R_2^3} \frac{1}{N} \sum_{j=1}^{N} (m - R_1)_j^3,$$

$$R_4 = \frac{1}{R_2^4} \frac{1}{N} \sum_{j=1}^{N} (m - R_1)_j^4, \quad \textbf{(14)}$$

where N is the number of CCD camera pixels.

4. ANALYSIS AND DISCUSSION OF THE EXPERIMENTAL DATA

Figure 2 presents the set of experimentally measured coordinate distributions of polarization ellipticities of laser images (the regime of polarization mapping, $\lambda = 0.63$ µm) of blood plasma films of group 1 [Figs. 2(a) and 2(b)], group 2 [Figs. 2(c) and 2(d)] and group 3 [Figs. 2(e) and 2(f)].

The comparative analysis of the obtained data shows an individual and rather similar statistical [Figs. 2(d)–2(f)] structure of the coordinate distributions of polarization ellipticity [Figs. 2(a)–2(c)] of laser images of the samples from all groups. This statement is proved by the similarity of histograms $N(\beta)$ of distributions β with localized main extrema. The quantitative differences between ellipticity maps of the samples of group 1, group 2, and group 3 are illustrated in Table 1.
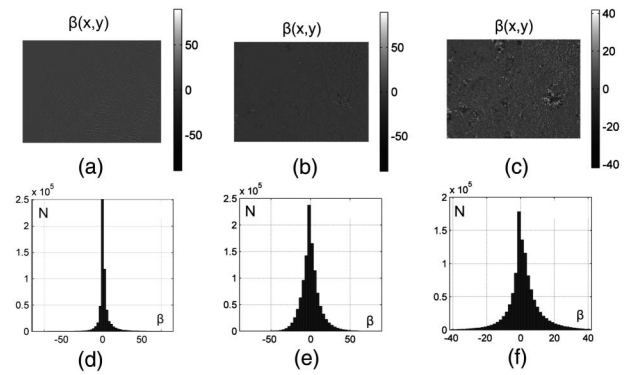

Fig. 2. Coordinate distributions of ellipticities of laser images ($\lambda = 0.63$ µm) of blood plasma films of (a), (d) group 1; (b), (e) group 2; and (c), (f) group 3. See explanations in the text.

It can be seen from the data obtained that the statistical moments of the 3rd and 4th orders proved to be the most sensitive in the task of differentiation of polarization maps of the samples of all groups. The differences between them are the following: 1.12–1.59 times for R_3 and 1.22–1.87 times for R_4.

For the considered groups ("1–2," "1–3," and "2–3") of blood plasma polycrystalline films, operational characteristics traditional for probative medicine [30–32] parameters were calculated: sensitivity (Se $= \frac{a}{a+b}100\%$), specificity (Sp $= \frac{c}{c+d}100\%$), and balanced accuracy (Ac $= \frac{\text{Se}+\text{Sp}}{2}$). Here, a and b are the number of correct and wrong diagnoses within group 2 and group 3, correspondingly; c and d are the same within group 1. Similar calculations were performed for groups 2 and 3 (see Table 2).

Table 1. Statistical ($R_{i=1;2;3;4}$) Moments of the 1st–4th Orders of the Distributions of Polarization Ellipticities of Laser Images ($\lambda = 0.63$ µm) of Blood Plasma of Group 1 (Healthy Donors), Group 2 (Nonalcoholic Fatty Liver Disease), and Group 3 (Chronic Hepatitis)

	$\beta(m \times n)$		
Parameters	Group 1	Group 2	Group 3
R_1	0.41 ± 0.028	0.45 ± 0.032	0.53 ± 0.041
R_2	0.12 ± 0.007	0.14 ± 0.008	0.17 ± 0.011
R_3	0.73 ± 0.057	0.82 ± 0.064	1.16 ± 0.094
R_4	1.02 ± 0.075	1.24 ± 0.09	1.91 ± 0.11

Table 2. Balanced Accuracies of the Method of Polarization Mapping ($\lambda = 0.6328$ µm) of Blood Plasma Samples

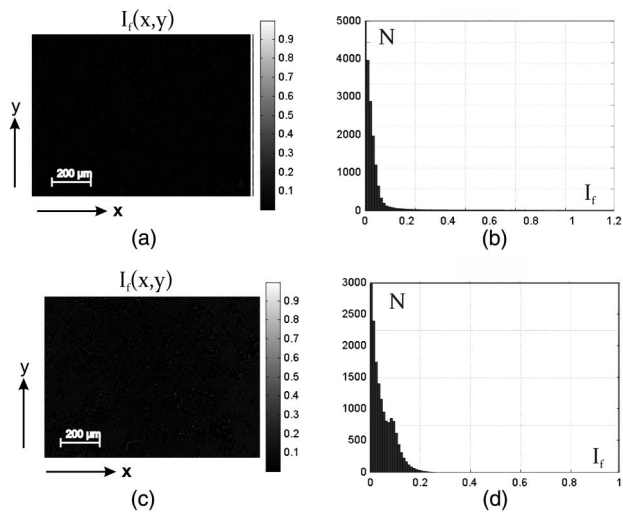| R_i	Ac (Group 1– Group 2) (%)	Ac (Group 1– Group 3) (%)	Ac (Group 2– Group 3) (%)
R_1	52	58	54
R_2	59	66	63
R_3	69	73	71
R_4	71	77	73

Fig. 3. (a), (c) Autofluorescence (0.63–0.67 μm) intensity maps and (b), (d) the corresponding histograms of the samples of polycrystalline films of blood plasma (group 1) for the following polarization states of probing beam: (a), (b) $\alpha_0 = 0°$; (c), (d) $\alpha_0 = \alpha_0^*$. See explanations in the text.

Fig. 5. (a), (c) Autofluorescence (0.63–0.67 μm) intensity maps and (b), (d) the corresponding histograms of the samples of polycrystalline films of blood plasma (group 3) for the following polarization states of probing beam: (a), (b) $\alpha_0 = 0°$; (c), (d) $\alpha_0 = \alpha_0^*$. See explanations in the text.

Thus, the statistical analysis of distributions of polarization ellipticity conditioned by the mechanisms of linear birefringence appeared to be not effective enough in the task of differential diagnostics of liver pathology severity degree.

The possibilities of the method of laser autofluorescence of polycrystalline networks of blood plasma films in red spectral region (0.63–0.67 μm) is illustrated in Figs. 3–5. One can see the coordinate distributions of autofluorescence intensity I [parts (a) and (c)], and histograms $N(I)$ [parts (b) and (d)] obtained for different polarization states of the probing beam of the blue laser ($\lambda = 0.405$ μm).
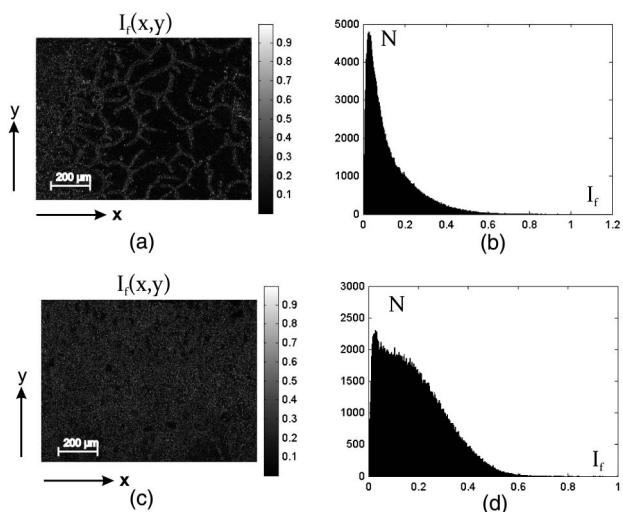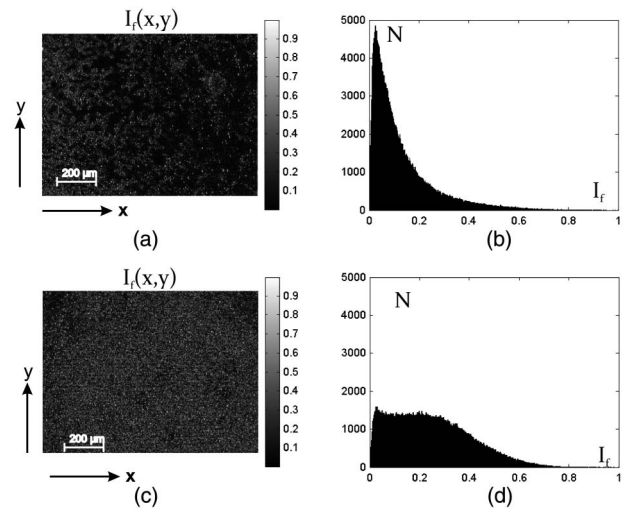

Fig. 4. (a), (c) Autofluorescence (0.63–0.67 μm) intensity maps and (b), (d) the corresponding histograms of the samples of polycrystalline films of blood plasma (group 2) for the following polarization states of probing beam: (a), (b) $\alpha_0 = 0°$; (c), (d) $\alpha_0 = \alpha_0^*$. See explanations in the text.

Analysis of the data presented in Figs. 3–5 revealed the sufficient dependence of laser autofluorescence (0.63–0.67 μm) of blood plasma polycrystalline films on the polarization state of the laser beam probing that reaches its extreme level [part (d)] for optimal polarization state α_0^* calculated using relation Eqs. (8)–(12).

The differences between the coordinate distribution of laser polarization intensity of autofluorescence $I(\alpha_0^*)$ of the protein networks of groups 1, 2, and 3 are quantitatively illustrated in Table 3.

The similar comparative investigations were performed for other (polarizationally nonoptimal) polarization states ($\alpha_0 = 0°$) of the probing laser beam. Exciting laser interference by the beam with polarization state α_0^* optimized using relation Eqs. (8)–(12) appeared to be the most diagnostically sensitive. During the process of research, the following quantitative criteria of differentiation of benign and malignant changes were determined: the difference between the values of the set of statistical moments of the 3rd and 4th orders characterizing the distributions $I(\alpha_0^*)$ make 1.48–3.82 times for R_3, 1.36–3.64 times for R_4.

Balanced accuracies of the method of laser polarization autofluorescence of porphyrins is shown in Table 4.

Table 3. Statistical ($R_{i=1;2;3;4}$) Moments of the 1st–4th Orders of the Distributions of Autofluorescence Intensities $I(\alpha_0^*)$ of Blood Plasma of Group 1, Group 2, and Group 3 in the Red Spectral Region (0.63–0.67 μm)

Parameters	$I(\alpha_0^*)$		
	Group 1	Group 2	Group 3
R_1	0.08 ± 0.005	0.11 ± 0.006	0.27 ± 0.013
R_2	0.06 ± 0.004	0.09 ± 0.005	0.18 ± 0.014
R_3	0.29 ± 0.017	0.43 ± 0.034	1.11 ± 0.084
R_4	2.37 ± 0.18	1.74 ± 0.12	0.65 ± 0.0049

Table 4.   Balanced Accuracies of the Method of Autofluorescence Mapping of Blood Plasma Samples B in the Red Spectral Region (0.63–0.67 µm)

R_i	Ac (Group 1–Group 2) (%)	Ac (Group 1–Group 3) (%)	Ac (Group 2–Group 3) (%)
R_1	83	90	89
R_2	81	92	85
R_3	88	94	92
R_4	90	96	94

Table 5.   Balanced Accuracies of the Method of Autofluorescence Mapping of Blood Plasma Samples in the Yellow–Green Spectral Region (0.5–0.53 µm)

R_i	Ac (Group 1–Group 2) (%)	Ac (Group 1–Group 3) (%)	Ac (Group 2–Group 3) (%)
R_1	71	76	73
R_2	77	81	79
R_3	82	85	84
R_4	83	89	86

In the "yellow–green" region (0.5–0.53 µm) of the autofluorescence spectrum of blood plasma films, similar investigations gave the results in Table 5.

Comparative analysis of the obtained data (Tables 4 and 5) showed excellent (Ac > 90%) and good (85% < Ac < 89%) quality of the test [33,34]) for the task of differential diagnostics of nonalcoholic fatty liver disease and chronic hepatitis.

5. CONCLUSION

1. It has been proposed that the model laser polarization autofluorescence of blood plasma polycrystalline films accounts for the mechanisms of amplitude and phase anisotropies.

2. It has been found that there is an interconnection between the statistical parameters of laser polarization autofluorescence and the peculiarities of the mechanisms of optically anisotropic absorption of blood plasma polycrystalline films.

3. It has been demonstrated that there is an efficiency in the method of Mueller-matrix mapping of laser polarization autofluorescence of blood plasma films in different spectral regions (0.5–0.53 µm and 0.63–0.67 µm) during the differentiation of nonalcoholic fatty liver disease and chronic hepatitis.

REFERENCES

1. J. M. Bueno and M. C. W. Campbell, "Polarization properties of the in vitro old human crystalline lens," Ophthalmic Physiol. Opt. **23**, 109–118 (2003).
2. T. T. Tower and R. T. Tranquillo, "Alignment maps of tissues: I. Microscopic elliptical polarimetry," Biophys. J. **81**, 2954–2963 (2001).
3. J. M. Bueno and J. Jaronski, "Spatially resolved polarization properties for in vitro corneas," Ophthalmic Physiol. Opt. **21**, 384–392 (2001).
4. T. T. Tower and R. T. Tranquillo, "Alignment maps of tissues: II. Fast harmonic analysis for imaging," Biophys. J. **81**, 2964–2971 (2001).
5. M. Shribak and R. Oldenbourg, "Techniques for fast and sensitive measurements of two-dimensional birefringence distributions," Appl. Opt. **42**, 3009–3017 (2003).
6. J. M. Bueno and F. Vargas-Martin, "Measurements of the corneal birefringence with a liquid-crystal imaging polariscope," Appl. Opt. **41**, 116–124 (2002).
7. M. H. Smith, P. Burke, A. Lompado, E. Tanner, and L. W. Hillman, "Mueller matrix imaging polarimetry in dermatology," Proc. SPIE **3991**, 210–216 (2000).
8. M. H. Smith, "Interpreting Mueller matrix images of tissues," Proc. SPIE **4257**, 82–89 (2001).
9. O. V. Angelsky, N. N. Dominikov, P. P. Maksimyak, and T. Tudor, "Experimental revealing of polarization waves," Appl. Opt. **38**, 3112–3117 (1999).
10. S. Lu and R. A. Chipman, "Interpretation of Mueller matrices based on polar decomposition," J. Opt. Soc. Am. A **13**, 1106–1113 (1996).
11. O. V. Angelsky, P. V. Polyanskii, and C. V. Felde, "The emerging field of correlation optics," Opt. Photon. News **23**(4), 25–29 (2012).
12. O. V. Angelsky and Y. A. Ushenko, "The degree of mutual anisotropy of biological liquid crystals net during the diagnostics of human tissues birefringence," Adv. Opt. Technol. **2010**, 321275 (2010).
13. Y. A. Ushenko, Y. Y. Tomka, and A. V. Dubolazov, "Laser diagnostics of anisotropy in birefringent networks of biological tissues in different physiological conditions," Quantum Electron. **41**, 170–175 (2011).
14. Y. O. Ushenko, Y. Y. Tomka, I. Z. Misevitch, V. V. Istratiy, and O. I. Telenga, "Complex degree of mutual anisotropy of biological liquid crystals nets," Opt. Eng. **50**, 039001 (2011).
15. Y. A. Ushenko, Y. Y. Tomka, A. V. Dubolazov, and O. Y. Telenga, "Diagnostics of optical anisotropy changes in biological tissues using Müller matrix," Quantum Electron. **41**, 273–277 (2011).
16. O. V. Angelsky, A. Y. Bekshaev, P. P. Maksimyak, A. P. Maksimyak, S. G. Hanson, and C. Y. Zenkova, "Self-diffraction of continuous laser radiation in a disperse medium with absorbing particles," Opt. Express **21**, 8922–8938 (2013).
17. O. V. Angelsky, C. Y. Zenkova, M. P. Gorsky, and N. V. Gorodyns'ka, "Feasibility of estimating the degree of coherence of waves at the near field," Appl. Opt. **48**, 2784–2788 (2009).
18. O. V. Angelsky, P. V. Polyanskii, I. I. Mokhun, C. Y. Zenkova, H. V. Bogatyryova, C. V. Felde, V. T. Bachinskiy, T. M. Boichuk, and A. G. Ushenko, Optical Measurements: Polarization and Coherence of Light Fields, Modern Metrology Concerns, L. Cocco, ed. (InTech, 2012), p. 458.
19. O. V. Angelsky, P. P. Maksimyak, and T. O. Perun, "Dimensionality in optical fields and signals," Appl. Opt. **32**, 6066–6071 (1993).
20. F. W. J. Teale and G. Weber, Ultraviolet fluorescence of the aromatic amino acids," Biochem. J. **65**, 476–482 (1957).
21. F. Teale, The ultraviolet fluorescence of proteins in neutral solution," Biochem. J. **76**, 381–388 (1960).
22. N. Nomura, S. Zolla-Pazner, M. Simberkoff, M. Kim, S. Sassa, and H. W. Lim, "Abnormal serum porphyrin levels in patients with the acquired immunodeficiency syndrome with or without hepatitis C virus infection," Arch. Dermatol. **132**, 906–910 (1996).
23. R. J. Hift, B. P. Davidson, C. van der Hooft, D. M. Meissner, and P. N. Meissner, "Plasma fluorescence scanning and fecal porphyrin analysis for the diagnosis of variegate porphyria: precise determination of sensitivity and specificity with detection of protoporphyrinogen oxidase mutations as a reference standard," Clin. Chem. **50**, 915–923 (2004).
24. L. C. Courrol, F. R. de Oliveira Silva, E. L. Coutinho, M. F. Piccoli, R. D. Mansano, N. D. Vieira Júnior, N. Schor, and M. H. Bellini, "Study of blood porphyrin spectral profile for diagnosis of tumor progression," J. Fluoresc. **17**, 289–292 (2007).
25. M. B. Poh-Fitzpatrick, "A plasma porphyrin fluorescence marker for variegate porphyria," Arch. Dermatol. **116**, 543–547 (1980).
26. D. E. Kleiner and E. M. Brunt, "Nonalcoholic fatty liver disease: pathologic patterns and biopsy evaluation in clinical research," Semin. Liver Dis. **32**, 3–13 (2012).
27. D. van Beek and B. Funaki, "Hemorrhage a complication of percutaneous liver biopsy," Semin. Interventional Radiol. **30**, 413–416 (2013).
28. A. A. Bravo, S. G. Sheth, and S. Chopra, "Liver biopsy," N. Engl. J. Med. **344**, 495–500 (2001).

29. L. D. Cassidy, "Basic concepts of statistical analysis for surgical research," J. Surg. Res. **128**, 199–206 (2005).

30. Y. A. Ushenko, A. V. Dubolazov, V. O. Balanetskaya, A. O. Karachevtsev, and V. A. Ushenko, "Wavelet-analysis of polarization maps of human blood plasma," Opt. Spectrosc. **113**, 332–343 (2012).

31. Y. A. Ushenko, P. O. Angelskii, A. V. Dubolazov, A. O. Karachevtsev, M. I. Sidor, O. P. Mintser, B. P. Oleinichenko, and L. I. Bizer, "Complex polarization-phase and spatial-frequency selections of laser images of blood-plasma films in diagnostics of changes in their polycrystalline structure," Opt. Spectrosc. **115**, 601–609 (2013).

32. Y. A. Ushenko, "Concerted spatial-frequency and polarization-phase filtering of laser images of polycrystalline networks of blood plasma smears," J. Biomed. Opt. **17**, 117005 (2012).

33. C. S. Davis, *Statistical Methods of the Analysis of Repeated Measurements* (Springer-Verlag, 2002), p. 744.

34. A. Petrie and B. Sabin, *Medical Statistics at a Glance* (Blackwell, 2005), p. 157.